In Vivo Cytometry of Antigen-Specific T Cells Using ^{19}F MRI

Mangala Srinivas,[1] Michael S. Turner,[2] Jelena M. Janjic,[3] Penelope A. Morel,[2] David H. Laidlaw,[4] and Eric T. Ahrens[3,5]*

Noninvasive methods to image the trafficking of phenotypically defined immune cells are paramount as we attempt to understand adaptive immunity. A ^{19}F MRI-based methodology for tracking and quantifying cells of a defined phenotype is presented. These methods were applied to a murine inflammation model using antigen-specific T cells. The T cells that were intracellularly labeled ex vivo with a perfluoropolyether (PFPE) nanoemulsion and cells were transferred to a host receiving a localized inoculation of antigen. Longitudinal ^{19}F MRI over 21 days revealed a dynamic accumulation and clearance of T cells in the lymph node (LN) draining the antigen. The apparent T-cell numbers were calculated in the LN from the time-lapse ^{19}F MRI data. The effect of in vivo T-cell division on the ^{19}F MRI cell quantification accuracy was investigated using fluorescence assays. Overall, in vivo cytometry using PFPE labeling and ^{19}F MRI is broadly applicable to studies of whole-body cell biodistribution. Magn Reson Med 62:747–753, 2009. © 2009 Wiley-Liss, Inc.

Key words: in vivo cytometry; ^{19}F MRI; adaptive immunity; antigen-specific T cells; perfluoropolyether

The phenotype of an immune cell is defined by the patterns and expressions level of a lexicon of cell surface molecules (e.g., its CD antigens). These molecules are commonly assayed in vitro using techniques such as fluorescence activated cell sorting (FACS) or immunohistochemistry. Determining which cell surface molecules are present, and at what levels, under various culturing conditions or disease states is only one piece of the puzzle. A more difficult and equally important question to answer is: what biological role do these cell surface markers perform in vivo? Vital imaging of the trafficking patterns of phenotypically defined populations of immune cells, i.e., in vivo cytometry, can play a key role in answering this question.

T cells are key effectors of the immune system that are, paradoxically, involved in both fighting and causing disease. T cells are central to various inflammatory conditions including cancer, atherosclerosis, autoimmune disease, and transplant rejection. Moreover, several promising clinical trials have used adoptive transfer of T cells in cancer therapy (1–4). Visualization of the dynamic trafficking patterns of T cells in early and late phases of an immune response is paramount to understand the disease pathogenesis and the design of therapeutic interventions. The ability to perform in vivo cytometry in preclinical models, would allow for estimation of cell infiltration and persistence, as well as the assessment of dosage and delivery routes for potential therapies.

We present in vivo MRI methods for cell tracking. In our approach, cells of interest are labeled ex vivo with a "tracer" perfluoropolyether (PFPE) nanoemulsion, introduced into a subject, and cell migration is monitored using spin density-weighted ^{19}F MRI (5). The key advantage of this platform is that the ^{19}F images are specific for the labeled cells with no interference from the host's tissues.

The detection of PFPE-labeled cells using ^{19}F MRI or magnetic resonance spectroscopy is fundamentally different from prior methods for labeling and detecting cells with paramagnetic agents, such as with superparamagnetic iron oxide and related reagents (6–9). Cells labeled with metal ion-based contrast agents are detected indirectly via the agent's effect on the T_1, T_2, and/or T_2^* of surrounding ^{1}H in mobile water. Often, unambiguous identification of labeled cells and quantification of cell numbers in a region of interest (ROI) using these agents is challenged by the large ^{1}H background and intrinsic contrast.

In this study we use ^{19}F MRI to visualize and quantitate T-cell trafficking in a murine model of localized inflammation. We describe a novel PFPE nanoemulsion that is taken up by primary, T cells ex vivo without the need for transfection aids and without overt toxicity. Ovalbumin (ova)-specific T cells were harvested from D011.10 mice (10), labeled with nanoemulsion, and transferred to a recipient mouse with a focal ova inoculation. Using ^{19}F MRI we observed selective homing of the T cells to the proximal draining lymph node (DLN). We further demonstrate longitudinal quantification of the apparent T-cell numbers in the DLN directly from the in vivo MRI data. The contralateral lymph node (CLN) was used as a control for nonspecific T cell homing. Chemical modifications to the PFPE molecules permitted covalent binding of a fluorescent dye, enabling the formulation of a "dual mode" nanoemulsion (PFPE-Alexa647); we used this reagent to corroborate the MRI T-cell trafficking patterns by in vivo optical imaging. Moreover, we investigated the impact of in vivo

[1]Department of Tumor Immunology, Nijmegen Centre for Molecular Life Science, Radboud University Nijmegen Medical Centre, Nijmegen, Netherlands.

[2]Department of Immunology, University of Pittsburgh School of Medicine, Pittsburgh, Pennsylvania.

[3]Department of Biological Sciences, Carnegie Mellon University, Pittsburgh, Pennsylvania.

[4]Department of Computer Science, Brown University, Providence, Rhode Island.

[5]Pittsburgh NMR Center for Biomedical Research, Carnegie Mellon University, Pittsburgh, Pennsylvania.

Grant sponsor: National Institutes of Health; Grant numbers: R01-EB003453, R01-EB004155, and P01-HD047675; Grant sponsor: National Institute of Biomedical Imaging and Bioengineering to the Pittsburgh NMR Center as a National Biomedical Research Resource Center; Grant number: P41EB-001977.

*Correspondence to: Eric T. Ahrens, Department of Biological Sciences, Carnegie Mellon University, 4400 Fifth Ave., Pittsburgh, PA 15213. E-mail: eta@andrew.cmu.edu

Received 3 October 2008; revised 24 March 2009; accepted 2 April 2009.

DOI 10.1002/mrm.22063

Published online 7 July 2009 in Wiley InterScience (www.interscience.wiley.com).

T-cell division on the ^{19}F MRI cell quantification using carboxy-fluorescein diacetate succinimidyl ester (CFSE)-based cell labeling and FACS. Our results suggest that the PFPE ^{19}F MRI platform is a useful in vivo cellular imaging technique that can be applied to a wide variety of cell types and disease models. Additionally, the murine inflammation model described provides a platform to test the effect of antiinflammatory drugs or other therapies affecting cell trafficking.

MATERIALS AND METHODS

PFPE Nanoemulsion Synthesis

PFPE nanoemulsions were prepared using perfluorinated polyether (Exfluor, Round Rock, TX) with Pluronic L35 (Sigma-Aldrich, St. Louis, MO) in a 1:1 molar ratio. Emulsification was achieved by probe sonication using a Sonifier Cell Disruptor (Misonix, Farmingdale, NY) (11). Fluorescent versions of the PFPE polymers were synthesized as previously described (12). The fluorescent PFPE-Alexa647 was diluted in neat PFPE to obtain a final dye concentration at 0.05 mol% to PFPE and emulsified as above. For all emulsions the mean emulsion droplet diameter was 122 ± 17 nm as measured by dynamic light scattering using a Malvern Zetasizer Nano ZS (Malvern Instruments, Worcestershire, UK). The emulsion was prepared and 0.2 μm sterile-filtered on the same day as cell labeling.

T-cell Purification, Activation, and Labeling

T cells were purified from splenocytes obtained from DO11.10 donors using a MACS murine Pan T-cell isolation kit (Miltenyi Biotec, Auburn, CA). Cells were grown in Roswell Park Memorial Institute (RPMI) media with 10% fetal bovine serum (FBS), 100 μg/mL each of streptomycin and penicillin, and 1 μL/mL of 2-mercaptoethanol (Gibco-Invitrogen, Carlsbad, CA). Cells were activated in vitro by a 3-day incubation on anti-TCR coated plates, in the presence of 1 μg/mL anti-CD28 and 10 U/mL IL-2 (PeproTech, Rocky Hill, NJ). Cells were then harvested and resuspended in Hank's balanced salt solution (HBSS) at 5×10^6 per mL, with 1 μL/mL of 2-mercaptoethanol. The nanoemulsion was added to medium at 25 μL/mL (PFPE or PFPE-Alexa647), and the cells were incubated on ice for 10 min before addition of RPMI with 10% FBS and a further incubation of 1 hr at 37°C. Cells were washed in phosphate-buffered saline (PBS) containing 0.5% FBS twice and resuspended in 300 μL HBSS for transfer.

For cells labeled with CFSE (Invitrogen), activated T cells were suspended at 5×10^6 cells/mL in PBS with 0.5% FBS. Next, CFSE (5 μM) was added and the cells were incubated for 10 min at 37°C, followed by the addition of ice-cold RPMI with 10% FBS and a further incubation of 5 min on ice. The cells were then washed twice and resuspended in HBSS as before. Approximately 10^7 cells were used for each experiment, repeated in triplicate ($n = 3$).

Cellular Toxicity, Proliferation, and Phenotyping

For phenotypic analyses of labeled T cells, single cell suspensions were stained using either FITC, APC, Pacific Blue, PE, or PerCP-conjugated mAbs against CD25, DO11.10 TCR (KJ1-26), CD69, CD4 (BD PharMingen, Franklin Lakes, NJ), CD11c, and CCR7 (eBioscience, San Diego, CA). The expression levels of these markers were determined by FACS on an LSRII instrument (Becton Dickinson, Mountain View, CA).

Mouse Inflammation Model

T cells isolated from DO11.10 mice were labeled with PFPE or PFPE-Alexa647 nanoemulsion, or CFSE (Invitrogen), and injected intraperitoneally (i.p.) into three ($n = 3$) female MHC-compatible BALB/c (Jackson Laboratories, Bar Harbor, ME) mice (day 0). On the same day, mice received 50 μg chicken ova (Sigma Aldrich) or ova-Alexa647 conjugate (Invitrogen) in PBS, emulsified in Incomplete Freund's Adjuvant (IFA; Calbiochem-Novabiochem, La Jolla, CA) via a subcutaneous (s.c.) injection adjacent the quadriceps. Sterile PBS was injected on the contralateral side as a control. Additional control mice received either 1) ova/IFA s.c. and PFPE labeled T cells that were heat-killed by a 30-min incubation at 60°C, or 2) viable, PFPE-labeled T cells, but ova-free IFA s.c. Experiments were carried out in accordance with the guidelines provided by the Carnegie Mellon Institutional Animal Care and Use Committee (IACUC) and the National Institute of Health Guide for the Care and Use of Laboratory Animals.

NMR

^{19}F NMR on labeled tissues was carried out using a Bruker 500 MHz NMR spectrometer (Bruker BioSpin, Billerica, MA), with a calibrated trifluoroacetic acid (TFA) reference. For the labeled cell pellets, the average fluorine content per cell, F_c, was calculated by acquiring NMR spectra of a known number of PFPE-labeled cells ($\approx 10^6$) spiked with a known concentration of TFA. The F_c parameter was calculated from the integrated areas of the PFPE and TFA ^{19}F spectra.

In Vivo MRI

Prior to MRI, mice ($n = 3$) were anesthetized with an initial injection of ketamine/xylazine (50–100 mg/kg of ketamine and 5–10 mg/kg of xylazine), and an i.p. catheter was connected to a syringe pump (Harvard Apparatus, Hilliston, MA) to infuse the cocktail (13.6 mg/mL and 0.9 mg/mL, respectively, in saline) at 0.16 μL/hr for the session, with 0.2 μL/hr increments for the subsequent imaging sessions. Mice were intubated and connected to a mechanical ventilator (Harvard Apparatus) delivering a 1:2 mixture of oxygen and nitrous oxide at 140 strokes/min and 300 μL/stroke. An external reference containing PFPE nanoemulsion in H_2O at a concentration of 10^{19} fluorine atoms per mL was placed along the mouse's torso. MRI was carried out with an 11.7 T micro-imaging system equipped with a birdcage coil (Bruker). ^{19}F images were acquired using a RARE sequence with TR/TE = 1000/6.4 ms, a RARE factor of 8, and a 64×32 matrix. ^{1}H imaging was performed using a 2DFT spin-echo sequence with TR/TE = 1200/22 ms and a 512×256 matrix. Eight contiguous 5.0×2.8 cm (2-mm thick) slices were obtained, with the same coordinates for both ^{1}H and ^{19}F. The

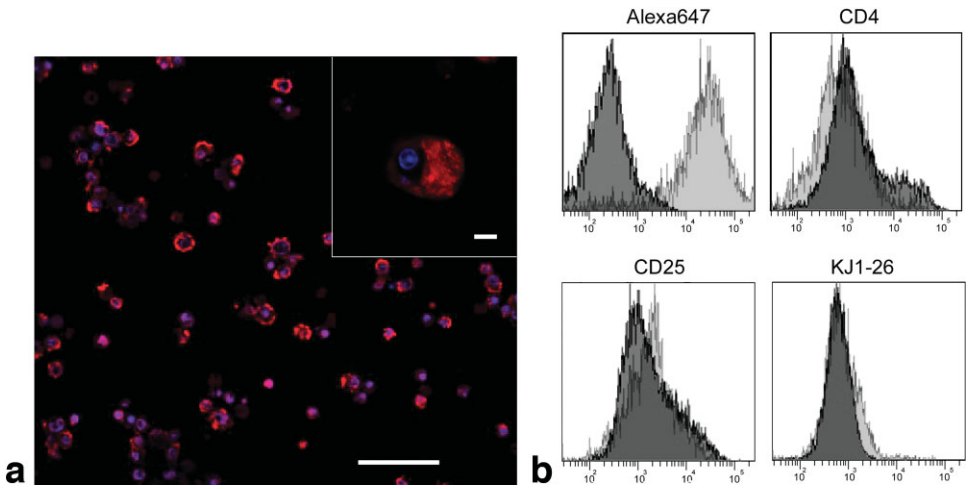

FIG. 1. Microscopy and FACS of PFPE-Alexa647 labeled T cells. **a:** Confocal image of labeled T cells immediately after labeling. Cell nuclei are stained in blue and the PFPE-Alexa647 is shown in red. Scale bar = 40 μm. The inset displays a single cell at high magnification, showing an apparent cytoplasmic distribution of the PFPE-Alexa647. Scale bar = 8 μm. **b:** FACS of labeled T cells immediately after PFPE labeling. The panels show the histograms of labeled T cells (light) and untreated control cells (dark) for the PFPE-Alexa647, CD4, CD25, and the ova-specific T-cell receptor, KJ1-26. No phenotypic differences were observed between labeled and untreated cells.

in vivo imaging was respiratory-gated, and the animal temperature was maintained at 37°C. The total time per imaging session was <2 hr. For display purposes, the ^{19}F images of the labeled cells were rendered in "hot-iron" pseudocolor and thresholded for ease of viewing against the ^{1}H underlay. We note that the thresholded resulted in an attenuation of the signal in the reference capillary.

The apparent number of PFPE-labeled cells was calculated directly from the in vivo MRI dataset, the external ^{19}F reference, and the measured F_c. The ^{19}F quantification was carried out using the raw, nonthresholded data. Based on anatomical data from the ^{1}H scans, ROIs were selected in slices containing visible ^{19}F signal. The ^{19}F signal per voxel was calculated, and we applied a Rician correction to increase the accuracy of apparent T-cell counts in low signal-to-noise ratio voxels as previously described (11). The same sealed capillary was used as a reference for all imaging experiments, thus any intrinsic SNR variation of the scanner among imaging sessions was compensated in the cell quantification analysis. The apparent T-cell numbers at different longitudinal timepoints were subjected to one-way analysis of variance (ANOVA), with a Tukey–Kramer multiple comparison post-test, using InStat software (GraphPad, La Jolla, CA).

T-cell Studies Using FACS

Control mice ($n = 3$) received CFSE-labeled T cells with an ova-Alexa647/IFA injection. Following injection, tissues from the DLN and site of injection were harvested. Single-cell suspensions were analyzed by FACS for the presence of the injected T cells by staining for the DO11.10 TCR (KJ1-26) and CD4. The uptake of ova-Alexa647 by resident DCs was assessed by staining for CD11c and Alexa647. The number of T cells in each tissue was calculated based on the fraction of the total number of cells that were $CD4^+$/$KJ1\text{-}26^+$ T cells. FACS results for the different time points were subjected to one-way ANOVA statistical analysis, with a Tukey–Kramer multiple comparison post-test.

In Vivo Fluorescence Imaging

Mice were anesthetized with ketamine/xylazine i.p. as above, and fur was removed over the lower portion of the animal by shaving and depilatory cream. In vivo optical images were acquired using a charge coupled camera (Photometrics, Tucson, AR) equipped with custom optics (Bioptechs, Butler, PA). Animals were illuminated using four quartz-halogen illuminators (Cuda Products, Jacksonville, FL). Excitation filters were 530/50 nm, and emission filters were 720/40 nm (Chroma Technologies, Brattleboro, VT). Imaging times were ≈10 sec, and black paper was used to mask autofluorescence from the gut. Mice were then sacrificed and the DLN and CLN extracted and again imaged.

Cell Microscopy

Confocal microscopy was carried out on PFPE-Alexa647 labeled T cells prepared as above. T cells were incubated on poly-L-lysine-coated glass coverslips for 30 min and fixed in 1% paraformaldehyde (PFA). The fixed cells were mounted in Vectashield (Vector Labs, Burlingame, CA) medium containing 4′-6-diamidino-2-phenylindole (DAPI). Cell imaging was performed using a Leica TCS SP2 spectral confocal microscope (Leica Microscopes, Exton, PA).

RESULTS

Characterization of Labeled T Cells

We confirmed an intracellular localization of the PFPE-Alexa647 nanoemulsion droplets using confocal microscopy in ova-specific T cells obtained from DO11.10 mice.

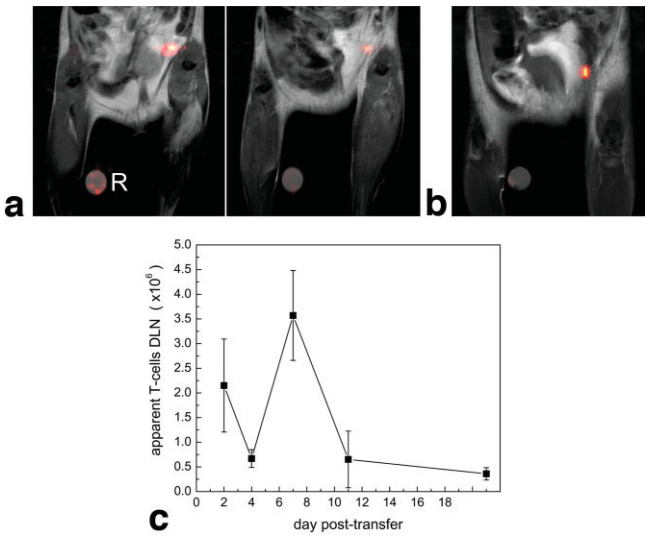

FIG. 2. Longitudinal in vivo MRI of PFPE-labeled T cells in the inflammation model. **a:** Representative images acquired at day 4 from a mouse that received PFPE-labeled T cells and ova/IFA. Shown are contiguous coronal slices where ^{19}F is rendered in pseudocolor and ^{1}H is in grayscale. T cells are detectable primarily in the DLN, and no labeled cells were detected in the CLN. The external reference capillary used for quantification is labeled *R.* **b:** Single slice from the same mouse at day 21. Some label is still detectable in the DLN, although the total integrated signal is ≈10-fold weaker than the maximum. **c:** Apparent T-cell quantification in DLN from in vivo MRI data. We calculated mean results for $n = 3$ animals and calculated errors bars from the standard deviation.

Figure 1a, acquired immediately after labeling, shows a distribution consistent with cytoplasmic localization that we confirmed at high magnification (Fig. 1a, inset). Figure 1a displays >95% labeling efficiency throughout the cell population, an observation supported by FACS analysis. Expression of the T-cell markers CD25, CD4, and the DO11.10 T-cell receptor (KJI-26) were not altered following PFPE labeling, as determined by FACS (Fig. 1b). We also performed quantitative analysis of ^{19}F NMR spectra from cell pellets to assay the mean PFPE loading factor per cell (F_c) and found $F_c = 1.7 \pm 0.9 \times 10^{12}$ ^{19}F/cell.

In Vivo T-cell Visualization and Quantification with MRI

Using longitudinal ^{19}F/^{1}H MRI, we followed the migration of ova-specific PFPE-labeled T cells in recipient mice given s.c. injections of ova/IFA. We observed a persistent, intense localization of T cells in the inguinal DLN on the side of antigen transfer. Figure 2a shows representative images at day 4. We did not detect PFPE-labeled T cells in the contralateral lymph node (CLN) node at any timepoint. However, we often observed faint ^{19}F signal in the mesenteric regions in certain animals. By day 21 the ^{19}F signal in the DLN was still detectable in single slices (Fig. 2b), but the integrated signals were substantially diminished (≈10-fold) from peak values, indicating gradual clearance. Assuming constant F_c, we calculated the apparent T-cell number in the DLN from the longitudinal data (Fig. 2c). The effects of any potential T-cell division and subsequent dilution of the nanoemulsion are not considered, thus the term "apparent" T-cell number is used. Our quantitative analysis revealed interesting dynamics of apparent T-cell recruitment to the DLN. We found that $2.1 \pm 0.9 \times 10^6$ apparent T cells reached the DLN at day 2, reaching a maximum of $3.6 \pm 0.9 \times 10^6$ at day 7 ($n = 3$ all days), followed by gradual clearance of the cells. Using a one-way ANOVA, we found extremely significant differences ($P = 0.0005$) in the apparent T-cell numbers among the different longitudinal timepoints. Specifically, pairwise comparisons between day 4 and day 7 ($P < 0.01$) and for day 7 versus days 11 and 21 ($P < 0.01$ and $P < 0.001$, respectively) show highly significant changes. Overall, these data show pronounced dynamical changes in apparent T-cell numbers for key stages of the cell trafficking, namely, homing and clearance.

The specificity of T-cell homing in our model was confirmed via two different in vivo controls (Fig. 3). Labeled, activated DO11.10 T cells were administered in the absence of ova (Fig. 3a); the cells failed to accumulate in the DLN but were visible in the mesenteric region. In addition, the observed ^{19}F signal from heat-killed PFPE-labeled T cells, in the presence of ova/IFA, appeared to concentrate in the mesenteric regions at day 2 (Fig. 3b), but thereafter was restricted to fatty tissue around the bladder. All ^{19}F signal observed in these regions was cleared by day 7 (not shown). Taken together, these data suggest that only the antigen-specific, viable T cells can reach the DLN, and only when antigen is present.

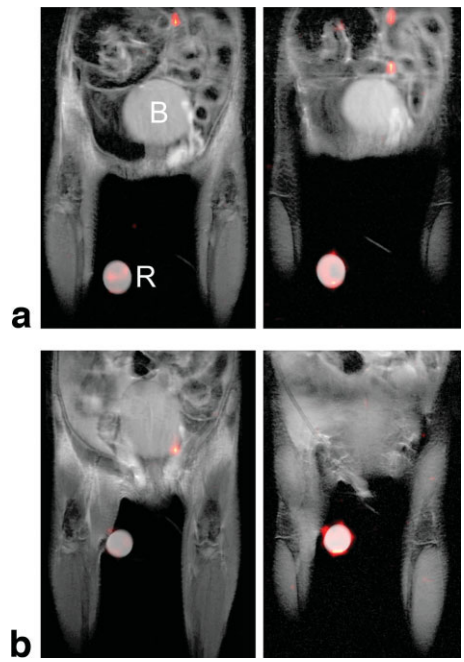

FIG. 3. In vivo MRI of T-cell trafficking controls. Shown are contiguous, coronal slices at day 4, rendered as in Fig. 2. **a:** Mouse inoculated with PFPE labeled T cells as before, but the host received antigen-free IFA. No T cells are detectable in the DLN. Instead, ^{19}F signal is detectable in the mesenteric region. The bladder is labeled *B*. **b:** Mouse received ova/IFA as before, but received PFPE-labeled, heat-killed T cells. No ^{19}F is visible in the DLN, but observed near the bladder at day 4.

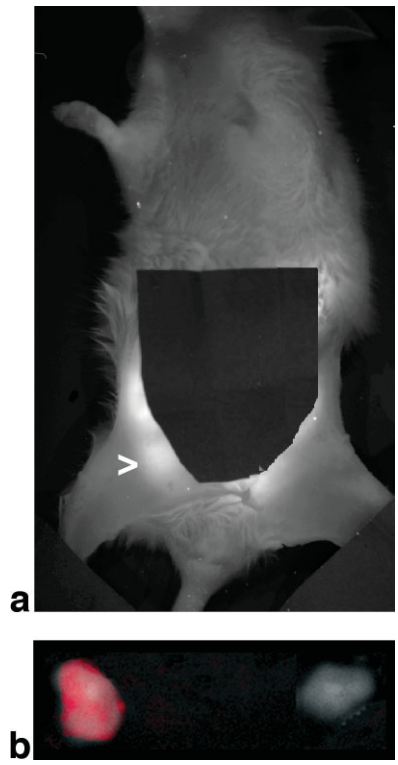

FIG. 4. Optical images showing PFPE-Alexa647-labeled T cells both in vivo and in excised tissue. **a:** In vivo fluorescence image at day 4 in a partially shaven mouse. Fluorescence is concentrated in the mesenteric region and the DLN (arrow). A mask was placed over the gut to reduce interference from the autofluorescent tissue. No fluorescence is visible in the CLN. **b:** Optical image of excised inguinal DLN and CLN. The image is an overlay of the fluorescent image (false color) and a white light image. The DLN (right) fluoresces and is visibly swollen compared to the CLN (left).

In Vivo Fluorescence Detection of T-cell Localization

We performed in vivo optical imaging in the inflammation model using T cells labeled with PFPE-Alexa647 conjugate. We observed bright fluorescence in the inguinal DLN (Fig. 4a). As a confirmation without background fluorescence from the mouse, we removed the inguinal DLN and CLN and imaged these separately (Fig. 4b); these data show a strong fluorescence signal in the DLN, while the CLN was nonfluorescent. We also performed FACS analysis of the T cells recovered from the DLN at day 4, and these data showed a mean intensity of Alexa647 of $\approx 10^2$ higher compared to the CLN (data not shown). Overall, the fluorescence experiments using PFPE-Alexa647 labeled T cells are consistent with the MRI findings.

FACS-Based Cell Tracking

In order to give insight into the dynamics of the apparent T-cell numbers quantified by MRI (Fig. 2), we used a CFSE-based cell assay in conjunction with FACS analysis. The magnitude of the fluorescence signal from CFSE-labeled cells decreases by half with each cell division, thus providing an assay of T-cell mitosis. CFSE has been used extensively for many in vivo and in vitro T-cell studies and is minimally toxic and does not affect proliferation (13). Additionally, an anti-DO11.10 TCR mAb (KJ1-26) allowed us to identify the injected DO11.10 T cells even after multiple divisions. DO11.10 T cells were labeled with CFSE prior to transfer to mice receiving ova/IFA. We also performed additional experiments in the same ova/IFA model, except ova-Alexa647 conjugate was used to track antigen from the site of injection using fluorescence detection. Mice ($n = 3$ for all timepoints) were sacrificed and the DLN and tissue at the site of antigen transfer were removed and processed for FACS at various timepoints out to 7 days.

Figure 5a shows representative FACS data of isolated cells from the DLN and the site of injection. The upper panels show staining for $CD11c^+$ dendritic cells (DCs) and ova-Alexa647 antigen; DCs carrying antigen were only observed at the site of injection. The largest number of $CD11c^+/Alexa647^+$ cells is seen at day 2 and decreased thereafter.

The injected T cells in the DLN and site of injection are also shown in Fig. 5a. Moderate numbers of cells with high levels of CFSE fluorescence are observed on day 2, peaking in the DLN on day 4. Figure 5b shows the mean fluorescence intensity of CFSE on gated $CD4^+/KJ1\text{-}26^+$ T cells and demonstrates a significant decrease between day 2 and day 4, suggesting that the cells proliferated during this period. Using a one-way ANOVA Tukey–Kramer test, $P < 0.001$ for the DLN and injection site for day 2 versus days 4 and 7. The level of CFSE remained constant after day 4, suggesting that no further proliferation occurred. We also estimated the absolute numbers of $CD4^+/KJ1\text{-}26^+$ T cells observed over time. Cells accumulated in the DLN and injection site (Fig. 5c). We note that FACS quantification of absolute T cells extracted from lymphoid organs is often prone to cell loss during tissue processing and thus inaccurate. Overall, FACS data show high levels of T-cell accumulation in the DLN, in agreement with the MRI.

DISCUSSION

In this article we describe novel PFPE cell labeling and ^{19}F MRI detection methods. We applied these methods to trafficking studies of antigen-specific T cells in a novel murine model of localized inflammation. From the longitudinal MRI data we calculated apparent T-cell numbers directly from the in vivo MR images, revealing targeted and dynamic T-cell homing. The in vivo trafficking data was corroborated with conventional CFSE-based cell labeling and FACS analysis on excised tissue.

The PFPE molecule has been shown to be nontoxic and is not degraded in cells (5,11,12). The carbon-fluorine bond is highly stable chemically; there are no known enzymes that degrade PFPE in vivo, and they do not degrade at typical lysosomal pH values (14,15). The perfluorocarbons are both lipophobic and hydrophobic and do not incorporate into cell membranes (14,15). Active exocytosis of the PFPE has not been observed in prior studies (5,11,12), but this remains a potential limitation of this cell-labeling technique. The ultimate clearance of PFPE agents from the body is believed to occur via the reticuloendothelial system and the lungs (16).

The T_1 of the PFPE is 437 ms at 11.7 T at atmospheric oxygen tension and 37°C (11), and because the spin-den-

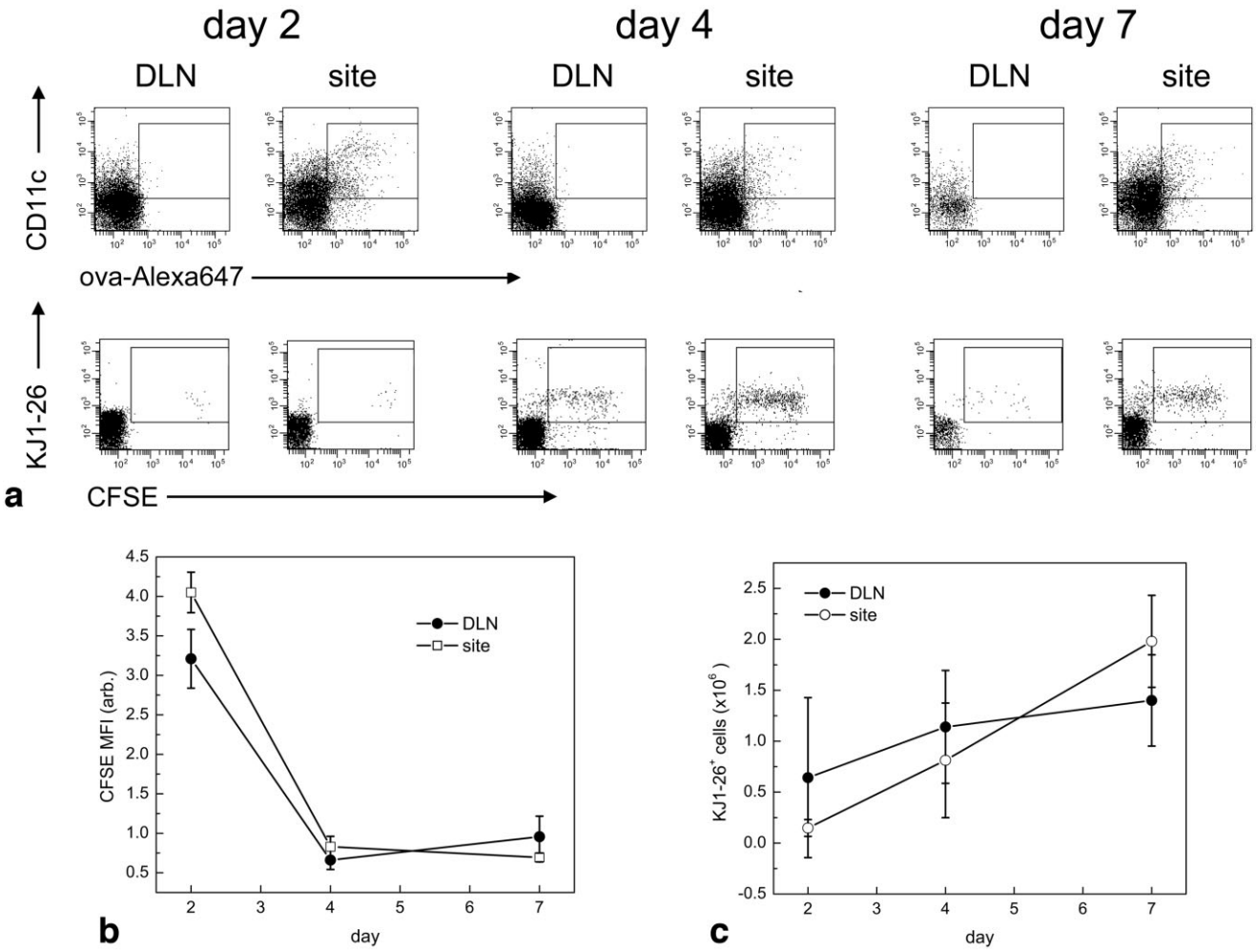

FIG. 5. FACS data from mice receiving CFSE-labeled T cells and ova-Alexa647. The FACS data were acquired by gating first on live cells and then either T cells or DCs. Representative data are shown ($n = 3$ for all timepoints). **a:** Dot plots showing CD11c and ova-Alexa647 (upper panels), KJ1-26 and CFSE (lower panels) from the DLNs, and tissue from the site of antigen transfer from days 2, 4, and 7. The gate windows used for these plots are shown. **b:** CFSE mean fluorescence intensity (MFI) for the DLN and site of antigen transfer over a 7-day period. The MFI drops significantly between days 2 to 4, indicative of rapid proliferation. Using an ANOVA Tukey–Kramer test, $P < 0.001$ for the DLN and injection site for day 2 versus days 4 and 7. **c:** The number of KJ1-26$^+$ T cells in the DLN and site of antigen transfer, estimated from the FACS analyses. The total number of LN cells was counted using a hemocytometer and the percent CD4$^+$/KJ1-26$^+$ cells was determined by FACS analysis as illustrated in panel **(a)**. The absolute number of KJ1-26$^+$ was determined by multiplying the total number of LN cells by the fraction expressing CD4$^+$ and KJ1-26$^+$.

sity-weighted MRI experiments were conducted using TR = 1000 ms, spins were mostly relaxed before each excitation. Furthermore, the same PFPE molecule was used in the external reference capillary; any residual T_1-weighting that was present in the ^{19}F images would be the same in both the cell-containing region and the reference capillary and thus does not affect quantification. Furthermore, due to the linear structure of the PFPE molecule, it has a low miscibility with oxygen, compared to, for example, cyclic perfluorocarbons such as perfluoro-15-crown-5 ether (17). Hence, pO2 variations are unlikely to affect quantification in our experiments.

Quantification of apparent T-cell numbers from MRI data (Fig. 2c) shows a maximum at day 7 followed by an ≈10-fold decline by day 21, indicating gradual clearance. In a previous trafficking study using FACS (18), activated, tumor antigen-specific T cells had peak cell numbers at tumor sites on day 7, reminiscent of the timing observed in our noninvasive MRI study. The same study (18) transferred 5×10^6 T cells into the tumor-bearing mice; they found that a large number of these cells, ≈80%, homed to lung metastases at day 6 posttransfer, using flow cytometric analyses. In comparison, we transferred 1×10^7 activated, antigen-specific cells and found ≈40% in the DLN at day 7. Our model did not involve a metastasizing tumor, and hence is expected to be less aggressive in T-cell recruitment. We note that our studies use activated T cells to minimize the possibility that endogenous T cells in the host mouse would be stimulated. In addition, activated T cells have upregulated proinflammatory adhesion molecules and preferentially traffic to sites of antigen deposition and inflammation in vivo (19,20).

The total ^{19}F content in an ROI can be measured accurately, and with knowledge of the PFPE content (F_c), the

apparent cell number can be calculated. For cells undergoing mitosis, this calculated value represents the actual cell number only at earlier times, and thereafter an accurate calculation of the absolute cell number content requires knowledge of the cell division rate in vivo. In vitro studies indicate that the intracellular F_c is halved with cell division. Measurement of total ^{19}F content in an ROI is not affected by cell division for nonitinerate cells. Dilution of label with cell division is a common scenario with many different cell-labeling modalities. Furthermore, dead cells and free (released) PFPE nanoemulsion can be scavenged by resident phagocytic leukocytes, possibly resulting in false-positives if substantial numbers of these phagocytes remain in the ^{19}F signal-positive voxels. Overall, the lower limit to cell detectability is $\approx 10^3-10^4$ cells per voxel (11,21).

To investigate T-cell division, cell trafficking, and potential cell death, we used CFSE dye and T-cell phenotypic markers with FACS analysis. We found that T cells present in the DLN had high levels of CFSE fluorescence at day 2, indicating that they had not yet proliferated. There was a dramatic drop in CFSE fluorescence by day 4 in the DLN, but remained stable thereafter (Fig. 5b). This would indicate that the cells underwent several rounds of proliferation between days 2 and 4, resulting in dilution of F_c. The FACS data suggested that the DO11.10 T cells continued to accumulate in the DLN between days 4 and 7.

Based on our data, we speculate that the transferred T cells initially traffic to all lymph nodes at the earliest timepoint, as expected for activated T cells. The T cells then preferentially accumulate in the DLN (Figs. 2, 4, 5). The MRI-observable drop in apparent T-cell number on day 4 (Fig. 2c) reflects rapid T-cell proliferation resulting in a swollen DLN and reduced F_c, followed by cell efflux from the DLN. Daughter cells leaving the DLN migrate to the site of antigen transfer (Fig. 5c), especially by day 7; this accumulation is not detectable by MRI due to the relatively low F_c in these cells, the result of repeated cell division. Indeed, at the injection site CFSE staining for KJ1-26$^+$ cells was very weak. By day 7, further influx of PFPE labeled T cells to the DLN occurs (Figs. 4c, 5), presumably from less-divided cells that remained in the blood circulation or other tissues, resulting in a peak in total ^{19}F content. The subsequent drop in signal in the DLN suggests that these cells then divide or die and are then cleared from the DLN by mechanisms that are yet to be elucidated.

Overall, the methods described herein can readily be adopted to study the trafficking of other cell types (e.g., stem cells (21,22)) or used for studies in a wide range of preclinical animal models. Moreover, the murine inflammation model we describe can be applied to studies of therapeutics, such as small molecules or recombinant proteins, that modulate immune cell trafficking.

ACKNOWLEDGMENT

We thank Patrizia Fuschiotti, Byron Ballou, Kevin Hitchens, Virgil Simplaceanu, Dewayne Falkner, and Chris Navara for valuable assistance.

REFERENCES

1. Mackensen A, Meidenbauer N, Vogl S, Laumer M, Berger J, Andreesen R. Phase I study of adoptive T-cell therapy using antigen-specific CD8(+) T cells for the treatment of patients with metastatic melanoma. J Clin Oncol 2006;24:5060–5069.
2. Kershaw MH, Westwood JA, Parker LL, Wang G, Eshhar Z, Mavroukakis SA, White DE, Wunderlich JR, Canevari S, Rogers-Freezer L, Chen CC, Yang JC, Rosenberg SA, Hwu P. A phase I study on adoptive immunotherapy using gene-modified T cells for ovarian cancer. Clin Cancer Res 2006;12:6106–6115.
3. Morgan RA, Dudley ME, Wunderlich JR, Hughes MS, Yang JC, Sherry RM, Royal RE, Topalian SL, Kammula US, Restifo NP, Zheng ZL, Nahvi A, de Vries CR, Rogers-Freezer LJ, Mavroukakis SA, Rosenberg SA. Cancer regression in patients after transfer of genetically engineered lymphocytes. Science 2006;314:126–129.
4. Porter DL, Levine BL, Bunin N, Stadtmauer EA, Luger SM, Goldstein S, Loren A, Phillips J, Nasta S, Perl A, Schuster S, Tsai D, Sohal A, Veloso E, Emerson S, June CH. A phase 1 trial of donor lymphocyte infusions expanded and activated ex vivo via CD3/CD28 costimulation. Blood 2006;107:1325–1331.
5. Ahrens ET, Flores R, Xu H, Morel PA. In vivo imaging platform for tracking immunotherapeutic cells. Nat Biotechnol 2005;23:983–987.
6. Arbab AS, Liu W, Frank JA. Cellular magnetic resonance imaging: current status and future prospects. Expert Rev Med Devices 2006;3:427–439.
7. Ho C, Hitchens TK. A non-invasive approach to detecting organ rejection by MRI: monitoring the accumulation of immune cells at the transplanted organ. Curr Pharm Biotechnol 2004;5:551–566.
8. Bulte JWM, Kraitchman DL. Iron oxide MR contrast agents for molecular and cellular imaging. NMR Biomed 2004;17:484–499.
9. Aime S, Barge A, Cabella C, Crich SG, Gianolio E. Targeting cells with MR imaging probes based on paramagnetic Gd(III) chelates. Curr Pharm Biotechnol 2004;5:509–518.
10. Robertson JM, Jensen PE, Evavold BD. DO11.10 and OT-II T cells recognize a C-terminal ovalbumin 323-339 epitope. J Immunol 2000;164:4706–4712.
11. Srinivas M, Morel PA, Ernst LA, Laidlaw DH, Ahrens ET. Fluorine-19 MRI for visualization and quantification of cell migration in a diabetes model. Magn Reson Med 2007;58:725–734.
12. Janjic JM, Srinivas M, Kadayakkara DKK, Ahrens ET. Self-delivering nanoemulsions for dual fluorine-19 MRI and fluorescence detection. J Am Chem Soc 2008;130:2832–2841.
13. Quah BJC, Warren HS, Parish CR. Monitoring lymphocyte proliferation in vitro and in vivo with the intracellular fluorescent dye carboxyfluorescein diacetate succinimidyl ester. Nat Prot 2007;2:2049–2056.
14. Krafft MP, Chittofrati A, Riess JG. Emulsions and microemulsions with a fluorocarbon phase. Curr Opin Colloid Interface Sci 2003;8:251–258.
15. Krafft MP. Fluorocarbons and fluorinated amphiphiles in drug delivery and biomedical research. Adv Drug Deliv Rev 2001;47:209–228.
16. Castro O, Nesbitt AE, Lyles D. Effect of a perfluorocarbon emulsion (Fluosol-DA) on reticuloendothelial system clearance function. Am J Hematol 1984;16:15–21.
17. Dardzinski BJ, Sotak CH. Rapid tissue oxygen tension mapping using 19F inversion-recovery echo-planar imaging of perfluoro-15-crown-5-ether. Magn Reson Med 1994;32:88–97.
18. Kjaergaard J, Peng L, Cohen PA, Shu S. Therapeutic efficacy of adoptive immunotherapy is predicated on in vivo antigen-specific proliferation of donor T cells. Clin Immunol 2003;108:8–20.
19. Rigby S, Dailey MO. Traffic of L-selectin-negative T cells to sites of inflammation. Eur J Immunol 2000;30:98–107.
20. Reinhardt RL, Khoruts A, Merica R, Zell T, Jenkins MK. Visualizing the generation of memory CD4 T cells in the whole body. Nature 2001;410:101–105.
21. Partlow KC, Chen J, Brant JA, Neubauer AM, Meyerrose TE, Creer MH, Nolta JA, Caruthers SD, Lanza GM, Wickline SA. 19F magnetic resonance imaging for stem/progenitor cell tracking with multiple unique perfluorocarbon nanobeacons. FASEB J 2007;21:1647–1654.
22. Ruiz-Cabello J, Walczak P, Kedziorek DA, Chacko VP, Schmieder AH, Wickline SA, Lanza GM, Bulte JWM. In vivo "hot spot" MR imaging of neural stem cells using fluorinated nanoparticles. Magn Reson Med 2008;60:1506–1511.